Inorganic Chemistry

Article

Solid-State Structural Characterization of a Rigid Framework of Lacunary Heteropolyniobates

May Nyman,*,† Aaron J. Celestian,‡ John B. Parise,‡ Gregory P. Holland,† and Todd M. Alam†

Sandia National Laboratories, P.O. Box 5800, Albuquerque, New Mexico 87185, and Center for Environmental and Molecular Sciences, Department of Geosciences, State University of New York, Stony Brook, New York 11794-2100

In our ongoing investigations of heteropolyniobate chemistry, a phase featuring decorated, A-type trivacant α-Keggin ions linked by their charge-balancing sodium cations has been isolated and structurally characterized. This is the first heteropolyniobate reported that has a true lacunary structure type. $Na_{15}[(PO_2)_3PNb_9O_{34}] \cdot 22H_2O$ (**1**) [triclinic space group $P\bar{1}$ (No. 2); $a = 12.242$ (2) Å, $b = 12.291$ (3) Å, $c = 22.056$ (4) Å; $\alpha = 93.12$ (3)°, $\beta = 99.78$ (3)°, $\gamma = 119.84$ (3)°; $Z = 4$, $V = 2799.2$ (10) Å³] is composed of bilayers of the heteropolyanions alternating with layers of hydrated Na^+ cations. Sodium cations also bridge the clusters within their layers through $Na-O_t-Nb$, $Na-O_b-Nb_2$, and $Na-O_t-P$ bonds (t = terminal and b = bridging). This phase is poorly soluble in water, suggesting that it is more characteristic of a framework of linked heteropolyanions rather than a water-soluble heteropolyanion salt. Two-dimensional solid-state ^{23}Na multiple-quantum magic angle spinning (MAS) NMR of **1** reveals five distinctive chemical and structural environments for sodium, which agrees with the crystallographic data. The ^{23}Na and ^1H MAS NMR studies further illustrate the rigid and immobile nature of this framework of cations and anions.

Introduction

Until around the turn of the 21st century, heteropolyniobate chemistry was virtually unknown; unlike its polyoxometalate (POM) cousins, heteropolyvanadates, -tungstates, and -molybdates, whose chemistries have been explored since the late 1800s (especially W and Mo).[1,2] As we continue to investigate polyoxoniobate chemistry and characterize new phases featuring polyanion clusters,[3–6] the similarities and differences between the W/Mo and Nb POM families become apparent. Some of the most important differences include the following. Basic conditions are always required for the synthesis and stability of the niobates, while acidic conditions are usually necessary for the synthesis and stability of the tungstates and molybdates. This is most likely because the niobate clusters possess higher negative charges because Nb is always pentavalent under these synthesis conditions whereas the tungstate and molybdate clusters contain predominantly hexavalent W/Mo. However, the synthesis of the W/Mo lacunary derivatives requires more basic processing conditions because these clusters possess higher charges.

The heteropolyniobate clusters have thus far only been obtained at elevated temperatures (hydrothermal); only the isopolyanions $[Nb_6O_{19}]^{8-}$ [7] and $[Nb_{10}O_{28}]^{6-}$ [8] have been isolated without hydrothermal processing. The niobates are electrochemically inert, while the molybdates and tungstates (and vanadates) have rich redox chemistries. Heteropolyniobates tend toward crystallization as insoluble or poorly soluble framework compounds composed of linked clusters, bridged by the alkali metals or more "traditional" framework polyhedra such as TiO_6 or NbO_6.[3–5] The tendency of the niobates toward these linked cluster compounds is perhaps a mechanism to stabilize the highly charged clusters because

* To whom correspondence should be addressed. E-mail: mdnyman@sandia.gov.

† Sandia National Laboratories.

‡ State University of New York.

(1) Baker, L. C. W.; Glick, D. C. *Chem. Rev.* **1998**, *98*, 3–50.

(2) Pope, M. T. *Heteropoly and Isopoly Oxometalates*; Springer-Verlag: New York, 1983.

(3) Bonhomme, F.; Larentzos, J. P.; Alam, T. M.; Maginn, E. J.; Nyman, M. *Inorg. Chem.* **2005**, *44*, 1774–1785.

(4) Nyman, M.; Bonhomme, F.; Alam, T. M.; Parise, J. B.; Vaughan, G. M. B. *Angew. Chem., Int. Ed.* **2004**, *43*, 2787–2792.

(5) Nyman, M.; Bonhomme, F.; Alam, T. M.; Rodriguez, M. A.; Cherry, B. R.; Krumhansl, J. L.; Nenoff, T. M.; Sattler, A. M. *Science* **2002**, *297*, 996–998.

(6) Nyman, M.; Criscenti, L. J.; Bonhomme, F.; Rodriguez, M. A.; Cygan, R. T. *J. Solid State Chem.* **2003**, *176*, 111–119.

(7) Goiffon, A.; Philippot, E.; Maurin, M. *Rev. Chim. Miner.* **1980**, *17*, 466.

(8) Graeber, E. J.; Morosin, B. *Acta Crystallogr.* **1977**, *B33*, 2137–2143.

the linkages always involve positively charged species (i.e., $[Ti_2O_2]^{4+}$ and $[Nb_2O_2]^{6+}$).[3] Alternatively, the predominance of linked clusters observed in polyoxoniobate chemistry may simply be favored by hydrothermal processing, as has been observed in hydrothermal synthesis of inorganic and organic–inorganic linked frameworks of heteropolyvanadates and -molybdates[9–23] and to a lesser extent the heteropolytungstates.[24] In either case, frameworks of linked clusters currently dominate heteropolyniobate chemistry, and hydrothermal synthesis is the only route thus far that has produced these clusters in sufficient yield and purity necessary for isolation and characterization.

Despite the differences between polyoxoniobate chemistry and polyoxotungstate and -molybdate chemistries, cluster geometries of polyoxoniobates have proven to be similar to those of the tungstates and molybdates. This is largely due to their similar ionic radii and preference for distorted octahedral coordination geometry (for hexacoordinate: $r(Nb^{5+})$ = 0.64 Å, $r(Mo^{6+})$ = 0.59 Å, and $r(W^{6+})$ = 0.60 Å).[25] The plenary α-Keggin ion $[PW_{12}O_{40}]^{3-}$ was the first structurally characterized heteropolyanion geometry,[26] and this cluster type, along with its lacunary derivatives, continues to be among the most commonly studied and exploited POM geometries.[2,27] Similarly, we have produced several examples of the dodecaniobate α-Keggin ion in phases featuring both isolated clusters and linked clusters.[3–5] A new heteropolyanion geometry that can be described as two fused, B-type trivacant lacunary α-Keggin ions has also been structurally characterized.[5]

In this report, we present the synthesis and solid-state characterization of $Na_{15}[(PO_2)_3PNb_9O_{34}]\cdot22H_2O$ (1), featuring a PO_2^+-decorated, A-type trivacant α-Keggin ion linked by charge-balancing sodium cations. Structural and chemical studies of this phase further enhance our knowledge of polyoxoniobate chemistry, as well as confirm some of the generalities observed thus far in this emerging family of POM compounds. Regarding the solid-state structure of 1, the cluster geometry resembles that of a previously reported tungstate cluster.[28] Similar to other heteropolyniobate phases, we observe a poor solubility behavior of this compound in which the clusters are linked together in the solid state by sodium cations only. The solid-state ^{23}Na magic angle spinning (MAS) NMR studies of 1 reveal remarkably distinctive sodium sites that are predominantly rigid, framework-like environments.

Experimental Section

General Instrumentation. X-ray powder diffraction was performed with a Bruker D8 Advance diffractometer in Bragg–Brentano geometry with Ni-filtered Cu Kα radiation. Infrared spectra (400–4000 cm^{-1}) were recorded on a Perkin-Elmer GX FTIR spectrum using the KBr pellet method. Samples were examined with a JEOL JSM-6300V scanning electron microscope equipped with a Link GEM Oxford detector and Iridium IXRF Systems software for energy-dispersive X-ray analysis. Thermal analysis was performed with a TA Instruments SDT 2960 for simultaneous thermogravimetric and differential thermal analysis (TGA–DTA) under a nitrogen flow with a heating rate of 5 °C/min.

Synthesis of $Na_{15}[(PO_2)_3PNb_9O_{34}]\cdot22H_2O$ (1). Sodium hexaniobate ($Na_7[HNb_6O_{19}]\cdot14H_2O$) was synthesized as previously reported.[7,29] Sodium pyrophosphate (Fisher, $Na_4[P_2O_7]\cdot10H_2O$, 0.89 g, 1.00 mmol of P) and sodium hexaniobate (0.43 g, 2.00 mmol of Nb) were combined in 2 mL of 1-butanol plus 6 mL of water in a 23-mL Teflon liner for a Parr reactor. The mixture was stirred for 20 min and placed in an oven at 150 °C for 15 h. Colorless lamellar crystals (up to 2 mm) were collected by vacuum filtration and rinsing with deionized water with a yield of ~0.4 g (78% based on Nb). Elemental analysis was performed by Galbraith Laboratories, Inc. (Knoxville, TN). The calculated average atomic weights agree with the experimental data: calculated, 35.7 wt % Nb, 5.3 wt % P, 14.7 wt % Na; found, 35.6 wt % Nb, 5.6 wt % P, 14.6 wt % Na. Likewise, the calculated weight percent of water agrees with the experimental data determined by thermogravimetry: 16.7% calculated and 16.9% found.

NMR Analysis. The solid-state ^{31}P MAS NMR spectra were obtained on a Bruker Advance 400 instrument at 162.0 MHz. The ^{31}P direct polarization (DP) and cross-polarization (CP) MAS NMR spectra were collected on a 4-mm broad-band MAS probe, spinning at 10 or 15 kHz, at 298 K. The ^{31}P DPMAS NMR spectra were obtained using a 20-s recycle delay, with a 4-μs π/2 pulse, and 64–256 scan averages. Complete ^{31}P CPMAS NMR buildup curves are presented in the Supporting Information, including experimental details. The ^{31}P NMR chemical shift was referenced to the secondary standard $H_2(NH_4)PO_4$ (δ = 0.8 ppm with respect to phosphoric acid at δ = 0 ppm). The high-speed ^1H MAS NMR spectra were obtained on a Bruker Advance instrument at a resonant frequency of 600.1 MHz utilizing a 2.5-mm broad-band probe with a spinning speed of 30 kHz, 4-s recycle delay, and 64 scan averages. The ^1H NMR chemical shifts were referenced to the secondary standard adamantine (δ = 1.63 ppm with respect to tetramethylsilane at δ = 0.0 ppm).

(9) Tripathi, A.; Hughbanks, T.; Tripathi, A. *J. Am. Chem. Soc.* **2003**, *125*, 10528–10529.
(10) Haushalter, R. C.; Lai, F. W. *Inorg. Chem.* **1989**, *28*, 2904–2905.
(11) Pan, C.-L.; Xu, J.-Q.; Chu, D.-Q.; Li, G.-H.; Lu, Z.-L.; Yang, G.-D. *Inorg. Chem. Commun.* **2003**, *6*, 939–941.
(12) Liu, C.-M.; Zhang, D.-Q.; Xiong, M.; Zhu, D.-B. *Chem. Commun.* **2002**, 1416–1417.
(13) Khan, M. I.; Yohannes, E.; Doedens, R. J. *Inorg. Chem.* **2003**, *42*, 3125–3129.
(14) Burkholder, E.; Zubieta, J. *Chem. Commun.* **2001**, 2056–2057.
(15) Duan, L.-M.; Pan, C.-L.; Xu, J.-Q.; Cui, X.-B.; Xie, F.-T.; Wang, T.-G. *Eur. J. Inorg. Chem.* **2003**, 2578–2581.
(16) Pan, C.-L.; Xu, J.-Q.; Li, G.-H.; Chu, D.-Q.; Wang, T.-G. *Eur. J. Inorg. Chem.* **2003**, 1514–1517.
(17) Bu, W.-M.; Ye, L.; Yang, G.-Y.; Gao, J.-S.; Fan, Y.-G.; Shao, M.-C.; Xu, J.-Q. *Inorg. Chem. Commun.* **2001**, *4*, 1–4.
(18) Lin, B.-Z.; Liu, S.-X. *Chem. Commun.* **2002**, 2126–2127.
(19) Leclaire, A.; Biot, C.; Rebbah, H.; Borel, M. M.; Raveau, B. *J. Mater. Chem.* **1998**, *8*, 439–444.
(20) Luan, G.; Wang, E.; Han, Z.; Li, Y. *Inorg. Chem. Commun.* **2001**, *4*, 541–543.
(21) Cui, X.-B.; Xu, J.-Q.; Sun, Y.-H.; Li, Y.; Ye, L.; Yang, G.-Y. *Inorg. Chem. Commun.* **2004**, *7*, 58–61.
(22) Shen, E.; Lu, J.; Li, Y.; Wang, E.; Hu, C.; Xu, L. *J. Solid State Chem.* **2004**, *177*, 4372–4376.
(23) Burkholder, E.; Zubieta, J. *Inorg. Chim. Acta* **2005**, *358*, 116–122.
(24) Lisnard, L.; Dolbecq, A.; Mialane, P.; Marrot, J.; Secheresse, F. *Inorg. Chim. Acta* **2004**, *357*, 845–852.
(25) Shannon, R. D. *Acta Crystallogr.* **1976**, *A32*, 751–767.
(26) Keggin, J. F. *Nature* **1933**, *131*, 908.
(27) Contant, R.; Herve, G. *Rev. Inorg. Chem.* **2002**, *22*, 63–111.

(28) Mazeaud, A.; Ammari, N.; Robert, F.; Thouvenot, R. *Angew. Chem., Int. Ed. Engl.* **1996**, *35*, 1961–1964.
(29) Alam, T. M.; Nyman, M.; Cherry, B. R.; Segall, J. M.; Lybarger, L. E. *J. Am. Chem. Soc.* **2004**, *126*, 5610–5620.

The one-dimensional (1D) ^{23}Na MAS NMR spectrum was acquired on a Bruker Advance 400 at 105.85-MHz spinning at a MAS frequency of 10 kHz at 298 K. A $\pi/6$ pulse of 0.5 μs was utilized to collect the 1D spectrum with 1024 scan averages and a 250-ms recycle delay. The chemical shift was referenced to a secondary 1 M aqueous solution of NaCl ($\delta = 0.0$ ppm). Two-dimensional (2D) ^{23}Na multiple-quantum (MQ)-MAS spectra were collected with a three-pulse z-filtered MQ-MAS pulse sequence utilizing a 3.7-μs excitation pulse, a 0.8-μs fast-amplitude-modulated[30−32] (FAM) conversion pulse, and a 20-μs z filter.[33] Three cycles for the FAM conversion pulse were optimal for the sample in this study. Phase cycling to select the (0, $\pm$3, 0, $-$1) coherence transfer pathway with phase-sensitive States[34] detection in F1 was used. Signal averaging of 960 scans, with a 250-ms recycle delay, were used for the 128 t_1 points. A shearing transform was performed following the conventional 2D Fourier transformation. The DMFIT software package was implemented to fit the resulting spectra and extract the quadrupolar parameters.[35]

Crystallography. Given the thin lamellar morphology of **1** and the difficulty in obtaining a large nontwinned single-crystal X-ray diffraction, data were collected on a MAR345 image-plate system using 1° ϕ rotations per frame at Beamline X7B of the National Synchrotron Light Source. Two sets of diffraction data were collected on a nontwinned single crystal to obtain first the weakly diffracting reflections and then the strongly diffracting reflections. The first set was exposed for 3 min/frame, the second set was exposed for 30 s/frame, and both sets were combined and rescaled for indexing and integration. Reflections were indexed, integrated, merged, and rescaled in the program DENZO and SCALEPACK.[36] The structure was solved by direct methods and refined by full matrix least squares in the program *SHELX97*.[37,38] Image-plate absorption corrections were performed using the method of Zaleski et al.[39] All fully occupied non-hydrogen atoms were refined anisotropically, while fractionally occupied water oxygens (O_w) were refined isotropically. Atoms labeled O50−O76 were treated as water molecules. Hydrogen sites of the water molecules could not be determined because of the low scattering power of hydrogen by X-rays. Crystallographic data are summarized in Table 1. Complete data of atomic coordinates and bond lengths and bond angles are available as a CIF file in the Supporting Information. Partial tables of atomic coordinates (Table 2), bond lengths (Tables 3 and 4), and bond angles (Table 3) are included here for clarity of discussion.

Discerning the difference between Na and O_w in X-ray scattering experiments proved nontrivial because of their similar X-ray scattering power and was further complicated by disorder and partial

Table 1. Summary of Crystallographic Data for **1**

formula	$H_{42}O_{62}P_4Nb_9Na_{15}$
fw	2340 g
space group	triclinic, $P\bar{1}$
unit cell parameters	$a = 12.242(2)$ Å
	$b = 12.291(3)$ Å
	$c = 22.056(4)$ Å
	$\alpha = 93.12(3)°$
	$\beta = 99.78(3)°$
	$\gamma = 119.84(3)°$
V	2799.2 (10) Å^3
Z	4
density (calc)	2.725 g/cm^3
synchrotron radiation	0.922 00 Å
exptl abs coeff, μ	2.141 mm^{-1}
temperature	293(2) K
2θ min, max	2.61°, 31.19°
morphology	plate
color	colorless
cryst dimens	$0.08 \times 0.08 \times 0.0015$ mm
measd reflns	7522
independent reflns	7522
reflns with $>2\sigma(I)$	7418
refinement on F^2	
R1 [$F^2 > 2\sigma(F^2)$]	0.0471
R1 (all data)	0.0474
wR2 (F^2)	0.1324
wR2 (all data)	0.1327
GOF	1.104
param refined	787

Table 2. Atomic Coordinates, Fractional Occupancies, and Atomic Displacement Parameters for Partially Occupied O_w (Water) Sites of **1**

atom	occupancy	x	y	z	U (Å^2)
O66	0.7	0.3138(19)	1.1248(19)	0.9398(9)	0.105(6)
O67	0.7	0.4473(13)	0.9491(13)	0.8510(6)	0.061(3)
O68	0.7	0.1757(18)	0.8394(18)	0.9402(8)	0.098(5)
O69	0.6	0.693(4)	0.582(4)	0.5486(17)	0.186(14)
O70	0.4	0.431(4)	0.361(4)	0.552(2)	0.144(15)
O71	0.5	0.467(4)	0.617(4)	0.552(2)	0.179(16)
O72	0.3	0.523(3)	0.951(3)	0.8817(14)	0.059(8)
O74	0.4	0.407(2)	1.152(2)	1.0349(11)	0.065(6)
O75	0.4	0.631(3)	0.978(3)	0.9261(13)	0.083(8)
O76	0.3	0.243(3)	0.958(3)	1.0117(13)	0.053(7)

occupancies. A combination of bond valance analysis, bonding geometry analysis, and chemical rationality was used to determine reasonable atom-type assignments to residual electron densities found in the Fourier difference maps. Assuming that Na bonds directly to the Keggin framework oxygens to maximize charge neutrality, all electron densities found within 2.1−2.9 Å from the framework oxygens were assigned as Na sites. This exercise revealed that the Keggin ion was surrounded by a shell of Na ions only on the closed side of the lacunary cluster (Na1−Na12, fully occupied sites). The next shell of electron density was assumed to be O_w sites. Bonds from sites found by Fourier difference electron density maps in the range of 2.3−2.9 Å were labeled as O_w, and no peaks were found at less than 2.1 Å from the Na sites. Three Fourier difference peaks were found in the lacunary hole. Two were assigned as Na13 and Na14 (also fully occupied) based on their geometries relative to the lacunary ion oxygens and bond valence sum (BVS) calculations. The third peak was designated as a water molecule that is bonded to both Na13 and Na14. Above the decorating phosphate groups, many difference peaks were found. One in particular stood as it was bonded to a phosphate group, which was assigned as Na15. The surrounding O_w sites were optimized at partial occupancies to avoid unreasonably close distances (<2.1 Å), to optimize BVS calculations for sodium, and to match the TGA data. The partially occupied O_w sites are summarized in Table 2.

(30) Madhu, P. K.; Goldbourt, A.; Frydman, L.; Vega, S. *Chem. Phys. Lett.* **1999**, *307*, 41.
(31) Madhu, P. K.; Goldbourt, A.; Frydman, L.; Vega, S. *J. Chem. Phys.* **2000**, *112*, 2377.
(32) Morais, C. M.; Lopes, M.; Fernandez, C.; Rocha, J. *Magn. Reson. Chem.* **2003**, *41*, 679.
(33) Amoreaux, J.-P.; Fernandez, C.; Steuernagel, S. *J. Magn. Reson. A* **1996**, *123*, 116.
(34) States, D. J.; Haberkorn, R. A.; Ruben, D. J. *J. Magn. Reson.* **1982**, *48*, 286.
(35) Massiot, D.; Fayon, F.; Capron, M.; King, I.; LeCalvé, S.; Alonso, B.; Durand, J.-O.; Bujoli, B.; Gan, Z.; Hoatson, G. *Magn. Reson. Chem.* **2002**, *40*, 70.
(36) Otwinowski, Z.; Minor, W. In *Methods in Enzymology, Macromolecular Crystallography*, 97-2 ed.; Carter, C. W., Sweet, R. M., Eds.; Academic Press: New York, 1997; Vol. 276.
(37) Sheldrick, G. M. *SHELX97*, 97-2 ed.; Institüt für Anorganische Chemie der Universität: Göttingen, Germany, 1998.
(38) Sheldrick, G. M. *Acta Crystallogr.* **1990**, *A46*, 467−473.
(39) Zaleski, J.; Wu, G.; Coppens, P. *J. Appl. Crystallogr.* **1998**, *31*, 302−304.

Table 3. Relevent Bond Angles (O$_1$–M–O$_2$, deg) and Distances (M–O$_a$, Å) of the [(PO$_2$)$_3$PNb$_9$O$_{34}$]$^{15-}$ Anion^a

	P$_d$1				P$_d$2				P$_d$3				P$_c$4		
O$_1$	distance	O$_2$	angle	O$_1$	distance	O$_2$	angle	O$_1$	distance	O$_2$	angle	O$_1$	distance	O$_2$	angle
O$_t$32	1.52(2)	O40	111.7(4)	O$_t$23	1.52 (1)	O25	112.3(3)	O$_t$31	1.52(1)	O34	111.6(3)	O$_b$12	1.52(2)	O13	110.3(3)
O$_t$40	1.52(2)	O21	109.9(3)	O$_t$25	1.52(2)	O24	108.5(3)	O$_t$34	1.53(4)	O29	110.2(3)	O$_b$13	1.54(5)	O19	109.6(3)
O$_b$21	1.56 (4)	O20	105.5(3)	O$_b$24	1.56 (4)	O23	110.3(3)	O$_b$29	1.57(2)	O31	109.5(3)	O$_b$19	1.54(2)	O12	109.8(3)
O$_b$20	1.57(2)	O32	109.5(3)	O$_b$33	1.56 (2)	O25	109.1(3)	O34		O30	110.6(3)	O$_b$16	1.55(2)	O12	109.1(3)
O40		O20	110.7(3)	O23		O33	110.1(3)	O29		O30	105.5(3)	O13		O16	109.0(3)
O32		O21	109.4(3)	O24		O33	106.4(3)	Ob30	1.57(2)	O31	109.3(3)	O19		O16	109.0(3)

	Nb1				Nb2				Nb3		
O$_1$	distance	O$_2$	angle	O$_1$	distance	O$_2$	angle	O$_1$	distance	O$_2$	angle
O$_t$17	1.75(6)	O5	102.4(2)	O$_t$26	1.75(3)	O14	102.1(3)	O$_t$18	1.77(2)	O11	101.2(2)
O$_b$5	1.96(2)	O14	92.0(2)	O$_b$14	1.97(6)	O6	92.1(2)	O$_b$11	1.91(2)	O10	93.8(2)
O$_b$14	1.98(2)	O4	87.9(2)	O$_b$6	1.98(2)	O26	99.3(3)	O$_b$10	1.95(5)	O18	98.7(2)
O$_b$4	2.01(3)	O17	100.0(2)	O$_b$28	2.02(7)	O28	99.1(3)	O$_b$39	1.98(6)	O39	102.4(2)
O$_b$3	2.03(2)	O17	101.4(2)	O$_b$7	2.03(5)	O26	101.5(2)	O$_b$21	2.15(6)	O18	93.8(2)
O$_c$16	2.47(8)	O5	72.8(2)	O$_c$16	2.46(3)	O14	72.7(2)	O$_c$12	2.41(2)	O11	86.6(2)
O17		O14	98.9(2)	O6		O28	88.3(2)	O11		O39	90.8(2)
O5		O3	88.6(2)	O14		O7	88.5(2)	O10		O21	85.3(2)
O4		O3	83.6(2)	O28		O7	83.5(2)	O39		O21	84.5(2)
O14		O16	72.5(2)	O6		O16	72.7(2)	O10		O12	82.7(2)
O4		O16	85.6(2)	O28		O16	86.8(2)	O39		O12	75.2(2)
O3		O16	87.8(2)	O7		O16	87.1(2)	O21		O12	78.4(2)

	Nb4				Nb5				Nb6		
O$_1$	distance	O$_2$	angle	O$_1$	distance	O$_2$	angle	O$_1$	distance	O$_2$	angle
O$_t$15	1.75(2)	O6	102.0(3)	O$_t$27	1.77(4)	O4	101.4(2)	O$_t$1	1.77(4)	O3	100.6(2)
O$_b$6	1.97(2)	O5	91.8(2)	O$_b$4	1.91(1)	O2	93.6(2)	O$_b$3	1.93(2)	O2	93.6(2)
O$_b$5	1.98(6)	O15	99.4(2)	O$_b$2	1.95(2)	O27	98.9(2)	O$_b$2	1.96(2)	O1	99.1(2)
O$_b$11	2.01(3)	O15	99.9(3)	O$_b$38	1.98(1)	O27	102.5(2)	O$_b$39	1.98(1)	O1	103.5(2)
O$_b$9	2.02(7)	O15	101.5(2)	O$_b$33	2.15(3)	O27	94.4(2)	O$_b$20	2.16(4)	O1	93.4(2)
O$_c$16	2.47(3)	O6	72.7(2)	O$_c$19	2.42(6)	O4	86.7(2)	O$_c$12	2.42(6)	O3	87.3(2)
O5		O11	88.2(2)	O4		O38	91.2(2)	O3		O39	90.8(2)
O6		O9	88.8(2)	O2		O33	84.8(2)	O2		O20	86.2(2)
O11		O9	83.3(2)	O38		O33	84.4(2)	O39		O20	83.8(2)
O5		O16	72.4(2)	O2		O19	82.5(2)	O2		O12	81.5(2)
O11		O16	86.3(2)	O38		O19	74.9(2)	O39		O12	74.9(2)
O9		O16	87.4(2)	O33		O19	77.5(2)	O20		O12	78.7(2)

	Nb7				Nb8				Nb9		
O$_1$	distance	O$_2$	angle	O$_1$	distance	O$_2$	angle	O$_1$	distance	O$_2$	angle
O$_t$8	1.76(1)	O7	100.8(2)	O$_t$37	1.76(2)	O9	100.6(2)	O$_t$35	1.77(2)	O28	100.9(3)
O$_b$7	1.93(1)	O22	94.0(2)	O$_b$9	1.93(4)	O10	93.6(2)	O$_b$28	1.91(4)	O22	93.8(2)
O$_b$22	1.95(5)	O8	98.4(2)	O$_b$10	1.95(2)	O37	98.9(2)	O$_b$22	1.96(3)	O35	99.3(2)
O$_b$38	1.99(6)	O8	103.4(2)	O$_b$36	1.99(1)	O37	102.5(2)	O$_b$36	1.97(1)	O35	102.9(2)
O$_b$24	2.16(7)	O8	94.0(2)	O$_b$30	2.15(3)	O37	93.6(2)	O$_b$29	2.16(4)	O35	93.6(2)
O$_c$19	2.41(2)	O7	87.7(2)	O$_c$13	2.39(2)	O9	87.3(2)	O$_c$13	2.43(2)	O28	86.9(2)
O7		O38	90.8(2)	O9		O36	90.5(2)	O28		O36	91.5(2)
O22		O24	85.7(2)	O10		O30	86.5(2)	O22		O29	84.8(2)
O38		O24	83.8(2)	O36		O30	84.0(2)	O36		O29	84.1(2)
O22		O19	82.1(2)	O10		O13	82.4(2)	O22		O13	81.9(2)
O38		O19	74.9(2)	O36		O13	75.3(2)	O36		O13	74.7(2)
O24		O19	77.5(2)	O30		O13	78.5(2)	O29		O13	78.5(2)

^{a} M = metal (Nb or P). Definitions: O$_t$ = terminal oxygen; O$_b$ = bridging oxygen; O$_c$ = central oxygen; P$_d$ = decorating phosphorus; P$_c$ = central phosphorus.

A Le Bail fit was performed on **1** using the *FULLPROF* suite of programs[40] and refined to a χ^2 of 4.3%. 2θ zero shift and unit cell parameters were allowed for refinement.
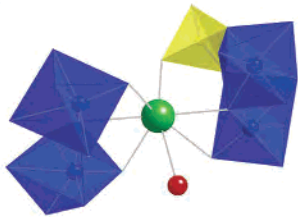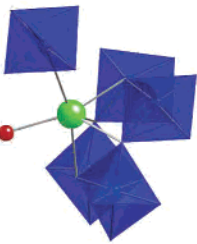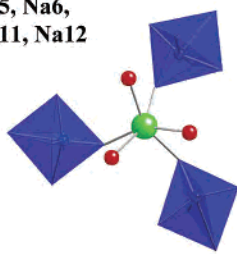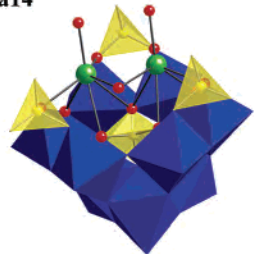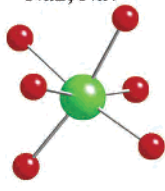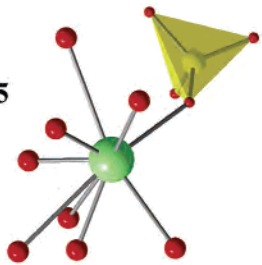
Results and Discussion

Synthesis of 1. Like the hydrothermal synthesis of any metastable phase, obtaining **1** in a pure form initially proved to be tricky in terms of the processing time, solution pH, solvent, and especially chemical precursors. We found that, under the conditions we investigated, this phase (or any other

(40) Rodriguez-Carvajal, J. FULLPROF: A Program for Rietveld Refine-ment and Pattern Matching Analysis. Abstracts from Satellite Meeting on Powder Diffraction of the XVth Congress of the IUCr, Toulouse, France, 1990.

PO$_4$-centered heteropolyniobates) could not be obtained using hydrous Nb$_2$O$_5$, the identified starting material for polyoxo-niobates reported previously.[4-6] Furthermore, the sodium salt of [P$_2$O$_7$]$^{4-}$ was the only phosphate precursor from which we could isolate PO$_4$-centered heteropolyniobates in the solid state for the hydrothermal and solvothermal conditions investigated. This observation may be due to the buffering behavior of phosphate ions; perhaps this phosphate salt provides an ideal alkalinity and pH for stabilization of PO$_4$-centered heteropolyniobates. The pH of the solution is around 10.5, which is in the 10.5–12.5 range that we observe to be optimal for the isolation of heteropolyniobate phases.[3,4] If a titanium alkoxide is added the the hydrothermal reaction (pH

Table 4. Na−O[a] Bonding Distances (Å) and Geometries in **1**

Na4, Na8, Na9

Na4		Na8		Na9	
O40	2.31(4)	O23	2.34(5)	O34	2.30(2)
O39	2.36(2)	O38	2.35(2)	O36	2.36(7)
O64	2.57(2)	O65	2.57(5)	O63	2.55(4)
O8	2.63(7)	O10	2.60(1)	O2	2.63(8)
O22	2.63(2)	O37	2.64(1)	O1	2.64(1)
O35	2.69(1)	O18	2.68(7)	O27	2.69(1)

Na1, Na3, Na10

Na1		Na3		Na10	
O15	2.33(1)	O26	2.32(3)	O17	2.32(6)
O9	2.46(3)	O7	2.46(8)	O3	2.47(3)
O28	2.49(3)	O4	2.49(3)	O11	2.48(8)
O6	2.52(8)	O14	2.53(3)	O5	2.53(3)
O36	2.58(3)	O38	2.58(3)	O39	2.57(3)
O63	2.65(7)	O65	2.62(4)	O64	2.64(4)

Na5, Na6, Na11, Na12

Na11

O61	2.36(3)
O60	2.36(8)
O59	2.39(3)
O1	2.41(6)
O37	2.43(5)
O8	2.43(4)

Na13, Na14

Na13

O66	2.28(3)
O29	2.54(6)
O22	2.60(4)
O24	2.64(2)
O67	2.67(3)
O13	2.77(3)
O19	2.81(9)

Na5		Na6		Na12	
O27	2.40(6)	O35	2.39(7)	O1	2.40(4)
O18	2.40(4)	O18	2.41(4)	O37	2.42(8)
O35	2.40(4)	O27	2.42(4)	O8	2.45(3)
O71	2.58(6)	O50	2.50(5)	O55	2.54(5)
O70	2.60(9)	O54	2.56(5)	O56	2.59(5)
O69	2.75(6)	O62	2.69(5)	O57	2.71(5)

Na14

O68	2.21(3)	O20	2.55(2)
O33	2.65(2)	O2	2.66(8)
O67	2.67(6)	O12	2.81(3)
O19	2.88(4)		

Na2, Na7

Na2		Na7	
O56	2.38(8)	O54	2.38(3)
O57	2.39(3)	O62	2.39(8)
O58	2.39(3)	O51	2.39(3)
O51	2.40(8)	O53	2.40(3)
O55	2.40(3)	O50	2.40(3)
O52	2.43(3)	O52	2.43(8)

Na15

Na15

O73	2.10(7)
O73	2.11(3)
O74	2.35(4)
O31	2.63(5)
O32	2.65(6)
O75	3.05(6)
O68	3.05(5)
O66	3.11(5)
O75	3.11(7)

[a] O1−O40 are lacunary cluster oxygens; O50−O76 are O_w, water oxygens. Red spheres represent water molecules (O_w); blue octahedra are NbO_6 of the cluster; yellow tetrahedra are PO_4 of the cluster.

= 11.8), $Na_{11}[Ti_2O_2][PNb_{12}O_{40}]\cdot xH_2O$ is the major product, a phase featuring chains of $[Ti_2O_2]^{4+}$-linked Keggin ions, isostructural with $Na_{12}[Ti_2O_2][TNb_{12}O_{40}]\cdot xH_2O$ and Na_{10}-$[Nb_2O_2][TNb_{12}O_{40}]\cdot xH_2O$ (T = Si and Ge) reported previously.[3] This phase cannot be formed using the analogous potassium precursors potassium hexaniobate and potassium pyrophosphate. We suspect that the two sodium cations bonded in the lacunary hole template stabilize this phase and the potassium cation is too large to function similarly. This is discussed further below in the description of the sodium sites.

Solution-state characterization of **1** by ^{31}P NMR was frustrated by either the lack of solubility or the aqueous instability of this phase. Solution-state ^{31}P NMR spectra were dominated by sharp PO_4 and P_2O_7 peaks, with some minor broader resonances that might be assigned to the lacunary anion of **1**. However, insufficient peak intensity due to the lack of sample solubility made this evaluation difficult. The peaks of PO_4 and P_2O_7 are probably due to the degradation of **1** in solution rather than minor impurities because these peaks do not show up in the solid-state NMR spectrum of **1**.

Solid-State Characterization of 1. A Le Bail fit was performed on the X-ray powder diffraction data of **1**. The results are shown in Figure 1. The powder diffraction spectrum of **1** shows a very high degree of preferred
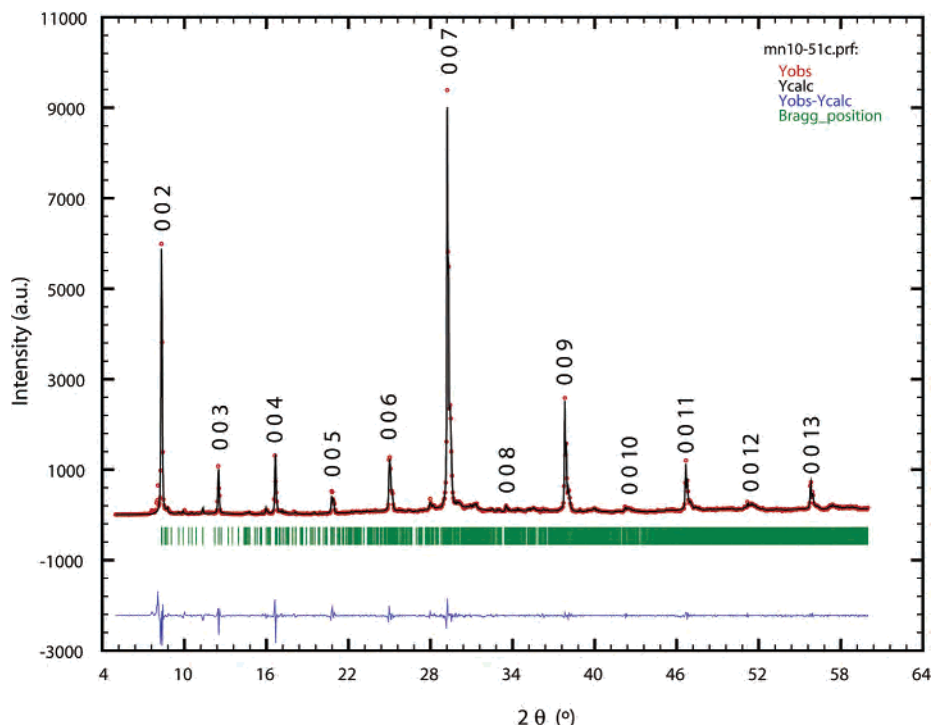
Figure 1. Observed, calculated, and difference spectra from a Le Bail fit of the powder X-ray diffraction data of **1**.
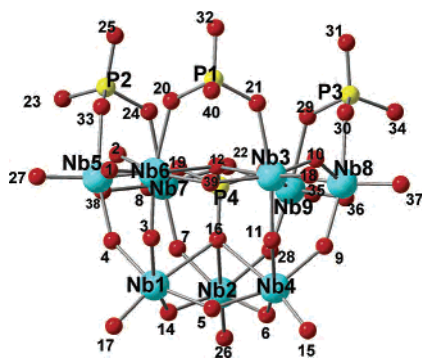

Figure 2. Labeled ball-and-stick model of the $[(PO_2)_3PNb_9O_{34}]^{15-}$ anion of **1**. Turquoise is niobium, yellow is phosphorus, and red is oxygen. The oxygen labels are represented by numbers only for ease of viewing the labels.

orientation on the 00*l* face because of the plate morphology of the crystals. Our attempts to remove the preferred orientation in the preparation of a sample for powder X-ray diffraction were unsuccessful. However, the Le Bail method proved that the structure determined by single-crystal X-ray diffraction was representative of the bulk, and no crystalline impurities were observed. Unit cell parameters by the Le Bail fit: $a = 12.215$ (3) Å, $b = 12.343$ (6) Å, $c = 21.804$ (9) Å, $\alpha = 92.70(4)°$, $\beta = 99.63(5)°$, and $\gamma = 119.97(2)°$. Unit cell parameters from single-crystal data: $a = 12.242$ (2) Å, $b = 12.291$ (3) Å, $c = 22.056$ (4) Å, $\alpha = 93.12(3)°$, $\beta = 99.78(3)°$, and $\gamma = 119.84(3)°$.

The $[(PO_2)_3PNb_9O_{34}]^{15-}$ cluster of **1** is described as an A-type trivacant lacunary α-Keggin ion decorated with three PO_4 tetrahedra, or PO_2^+ groups. Figure 2 shows the labeled ball-and-stick model of the $[(PO_2)_3PNb_9O_{34}]^{15-}$ lacunary ion, and relevant bond distances and bond angles for the anion are compiled in Table 3. Generally described, an A-type

trivacant cluster is formed by removing a triad of corner-sharing MO_6 (M = metal) octahedra from the plenary α-Keggin cluster.[41] Each of the decorating PO_4 tetrahedra shares two corners with the NbO_6 octahedra, and those two NbO_6 octahedra are edge-sharing. This cluster geometry was observed previously by Mazeaud et al. for organosilyl derivatives of the trivacant lacunary tungstate ion α-A-$[PW_9O_{34}(t\text{BuSiOH})_3]^{3-}$, in which $t\text{BuSiOH}^{2+}$ is the decorating group.[28] The NbO_6 octahedra exhibit distortion typical of polyoxoniobates, with a short terminal Nb−O bond trans to a long Nb−O bond and the Nb out-of-plane of the four axial oxygens. The ranges of observed bond lengths for the NbO_6 octahedra are Nb−O_t = 1.75−1.77 Å (t = terminal oxygen, bonded to one Nb), Nb−O_b = 1.91−2.16 Å (b = bridging oxygen, bonded to two Nb), Nb−O_c = 2.40−2.47 Å (c = central oxygen, bonded to two or three Nb and one P). The distortion is also exhibited in the octahedral O−Nb−O bond angles, ranging from 72 to 103°. The NbO_6 octahedra that are corner-sharing with the decorating PO_4 have additional bond distortion, with a Nb−O_b bond length around 2.2 Å that bridges to the phosphate, trans to a shorter Nb−O_b bond around 1.9 Å. Each decorating PO_4 has two terminal P−O_t bonds at ∼1.52 Å and two P−O_b bond lengths bridging to Nb with a bond distance of 1.56−1.57 Å. Tetrahedral O−P−O bond angles range from 105 to 112° for the decorating PO_4 tetrahedra. The lacunary clusters are hexagonally arranged in the crystal lattice in double layers in the *ab* plane, and these double layers alternate with hydrated sodium cations in the interlayer region (Figures 3 and 4). Additional sodium cations bridge the clusters by bonding to terminal and bridging oxygen atoms of the NbO_6 octahedra and PO_4 tetrahedra. The clusters are oriented such
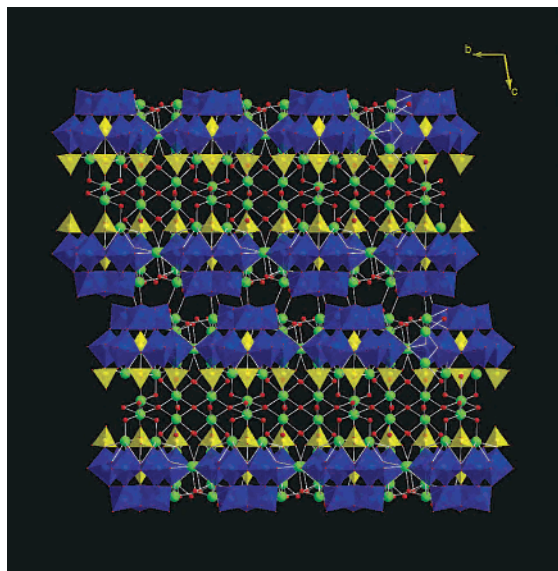
(41) Jeannin, Y. P. *Chem. Rev.* **1998**, *98*, 51−76.

Figure 3. View of **1** down the *y* axis showing the bilayers of A-type trivacant α-Keggin clusters sandwiching interlayer Na⁺ cations and lattice water. The blue octahedra are NbO_6, the yellow tetrahedra are PO_4, the red spheres are water molecules, and the green spheres are Na⁺ cations.
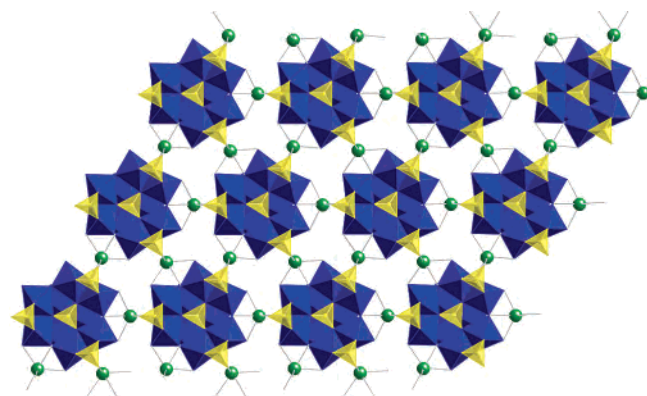

Figure 4. View of **1** down the *z* axis, emphasizing the hexagonal arrangement of the clusters in a single layer. The Na⁺ cations shown (green spheres) are Na4, Na8, and Na9, which link the clusters together in the *ab* plane.

that the decorating PO_4 tetrahedra point into the interlayer space. The two layers of clusters within a bilayer are laterally offset as A−B layers in a closest-packed array of spherical objects.

BVS calculations, TGA, and compositional analysis of **1** all support a chemical and structural model with no protons on the lacunary cluster, associated with neither the decorating PO_4 tetrahedra nor the NbO_6 octahedra. The ¹H and ³¹P MAS NMR results, however, suggest the presence of very strongly bound P−O−H_2O species. The high-speed (30-kHz) ¹H MAS NMR spectrum (Figure 1S in the Supporting Information) shows two resonances at $\delta = +5.8$ (96%) and +5.1 (3%) ppm. From ¹H double-quantum (DQ)-filtered MAS experiments (Figure 1S in the Supporting Information), it is seen that the resonance at $\delta = 5.0$ ppm is suppressed while the $\delta = +5.8$ ppm resonance is unaffected by the DQ filtering. From previously reported high-speed ¹H MAS NMR studies of H_2O and OH species in solid lattices containing phosphates,[42] the resonance at $\delta = +5.1$ ppm (3%) can be assigned to waters that are not strongly associated within
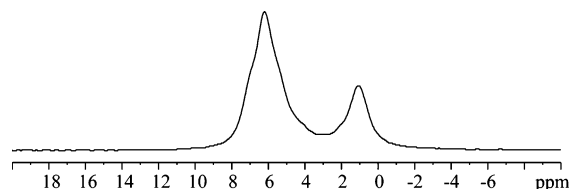

Figure 5. Solid-state ³¹P NMR spectrum of **1**. Two peaks in a 3:1 ratio at $\delta = +6.1$ and +1.4 ppm are assigned to the decorating PO_4 tetrahedra and the central PO_4 tetrahedron, respectively.

the "framework" of **1** and are sufficiently mobile to average the ¹H−¹H dipolar coupling within H_2O. The presence of a strong DQ signal for the peak at 5.8 ppm (96%) suggests that there is ¹H−¹H dipolar contact for these water molecules and that the protons are under exchange. On the basis of these observations, the ¹H resonance at $\delta = +5.8$ ppm (96%) represented water molecules that are strongly associated with the NbO_6 or PO_4 polyhedra of the lacunary clusters through hydrogen bonding. This is consistent with the structural information from X-ray data, in that nearly all water molecules are within the H-bonding distance from cluster oxygens (2.4−3.1 Å), many at a contact distance between 2.6 and 2.8 Å. The exception is O_w73, a fully occupied water oxygen site that is surrounded by partially and fully occupied O_w sites and Na13, Na14, and Na15. This site, which represents 4.5% of the water molecules, may correspond with the mobile water at 5.1 ppm (3%).

The solid-state ³¹P MAS NMR spectrum of **1** shown in Figure 5 agrees with the structure determined by single-crystal X-ray diffraction. The spectrum features two peaks in a 3:1 ratio at $\delta = +6.1$ and +1.4 ppm. The ¹H−³¹P CPMAS NMR experiments (see Figure 2S in the Supporting Information) showed a rapid preferential enhancement of the $\delta = +6.1$ ppm resonance, meaning that the decorating PO_4 tetrahedra have close spatial contact with a proton species (water closely associated with P=O). This rapid CP buildup is commonly observed in POH species within zeolites,[43] even though the POH ³¹P NMR chemical shifts are usually found at a slightly greater chemical shift ($\delta > 6$ ppm). On the basis of the ¹H MAS NMR results, the $\delta = +6.1$ ppm ³¹P NMR resonance is assigned to decorating PO_4 tetrahedra, which are strongly associated with H_2O. The $\delta = +6.1$ ppm resonance is asymmetric, with the asymmetry changing during the CPMAS experiments as a function of the CP contact time. This observation suggests that there are multiple unresolved resonances present at $\delta = +6.1$ ppm, which is consistent with the X-ray structure in that the three decorating PO_4 tetrahedra are inequivalent crystallographic sites. The slow ¹H−³¹P CP buildup (see the Supporting Information) of the $\delta = +1.4$ ppm peak supports the assignment of this resonance to the central PO_4 tetrahedron. No other ³¹P NMR resonances were observed, suggesting that there are no impurities or any minor phases containing phosphorus.

Finally, thermogravimetry also agreed with a structural model with no protons on the cluster. The weight loss due

(42) Alam, T. M.; Tischendorf, B. C.; Brow, R. K. *Solid State Nucl. Magn. Reson.* **2005**, *27*, 99−111.
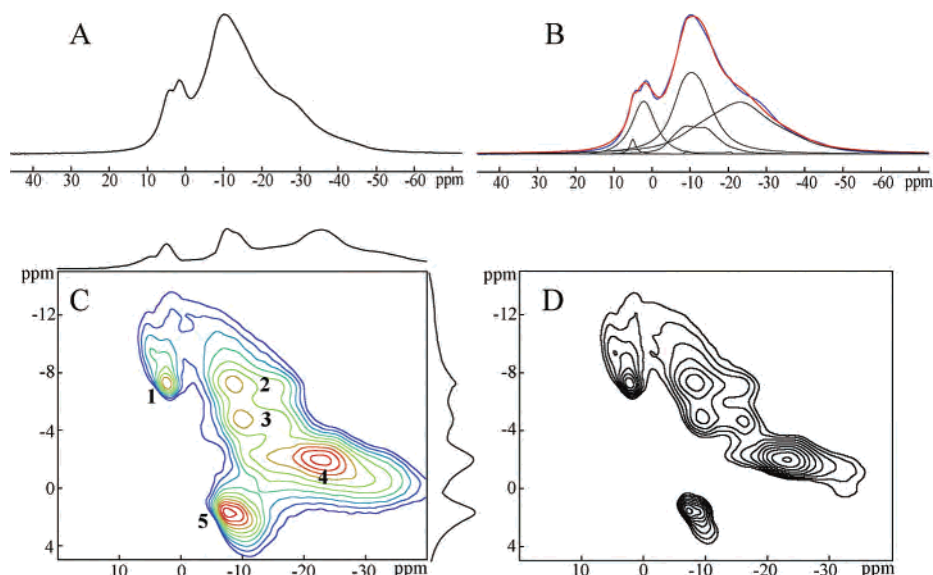(43) Kolodziejski, W.; Klinowski, J. *J. Phys. Chem., B* **1997**, *101*, 3937−3944.

Figure 6. (A) 1D ^{23}Na MAS NMR spectrum of **1**. (B) Simulated 1D ^{23}Na MAS NMR using the quadrupolar parameters (plus distributions in C_Q and δ_{iso}) presented in Table 5. (C) ^{23}Na MQ-MAS NMR spectrum of **1** with projections corresponding to sums across the isotropic (F1) and anisotropic (F2) dimensions. The different ^{23}Na sites are labeled. (D) Simulated ^{23}Na MQ-MAS NMR spectrum used to extract quadrupolar parameters (no distributions) presented in Table 5.

to water tails off around 400 °C. Weight loss due to a polyoxoniobate-bound proton usually occurs as a sharp weight loss between 500 and 600 °C. There are three distinct endothermic weight loss events observed in the TGA–DTA spectrum. The first, which accounts for about 50% of the weight loss, peaks at around 90 °C. The second event peaks at 145 °C and accounts for around 30% of the weight loss. The remaining 20% of weight loss occurs between 170 and 400 °C. An exothermic event around 550 °C corresponds with the crystallization of orthorhombic NaNbO$_3$ perovskite.

The 15 charge-balancing Na$^+$ cations per cluster are found in 15 fully occupied crystallographic sites. All Na–O bonds range from ∼2.1 to 3.0 Å, and the Na–O bonding information is summarized in Table 4 in the form of bond distances and graphic illustrations. O1–O40 are oxygens belonging to the lacunary cluster, and O50–O75 are water molecules, O$_w$. Na1–Na14 are all in regular and well-defined positions. Na4, Na8, and Na9 link the anionic clusters together within their hexagonally arranged layers. Each cluster is linked to its six nearest neighbors by these octahedrally coordinated sodium atoms, as shown in Figure 4. Each of these linking Na$^+$ cations bonds to two terminal (Nb–O$_t$) and one bridging (Nb–O$_b$–Nb) oxygen of one cluster and a phosphate terminal (P–O$_t$) oxygen, a bridging (Nb–O$_b$–Nb) oxygen, and a bridging (Nb–O$_b$–Nb) oxygen of a second cluster, with the seventh bond to a water oxygen, O$_w$. Na1, Na3, and Na10 sit in a four-ring window of one cluster and bond to a second cluster through a Na–O$_t$–Nb bond, and the sixth bond is to water. This four-ring window siting, in which Na$^+$ bonds to four Nb–O$_b$–Nb bridging oxygens, was also previously observed in sodium dodecaniobate Keggin phases.[3,4] Na5, Na6, Na11, and Na12 link three clusters in the *ab* plane through three Na–O$_t$–Nb bonds and are bonded to three water molecules. Na11 differs slightly from Na5, Na6, and Na12 in that the Na–O$_w$ bonds are shorter than the Na–O$_{framework}$ bonds for Na11. For Na5, Na6, and Na12, the Na–

O$_{framework}$ bonds are shorter than the Na–O$_w$ bonds. Na2 and Na7 are in very regular NaO$_6$ octahedra, coordinated to six O$_w$, and reside in the interlayer space. Na15 resides just above the open face of the lacunary cluster. It has one bond to P–O$_t$ of a decorating phosphate and is surrounded by six partially occupied water sites (fractional occupancy ranging from 0.3 to 0.7) and two fully occupied water sites, with Na–O$_w$ distances ranging from 2.1 to 2.8 Å. The very short Na–O$_w$ bonds ranging from 2.1 to 2.3 Å observed for Na15 and Na16 have likewise been observed in structures of other POM sodium salts.[44–46]

Finally, Na13 and Na14 sit just inside the belt of decorating PO$_4$ tetrahedra of the lacunary cluster. Each of these Na$^+$ cations is heptacoordinate, with one bond to bridging oxygen Nb–O$_b$–Nb, two bonds to bridging oxygens Nb–O$_b$–P, two bonds to the central μ^3 oxygens Nb$_2$–O$_c$–P, and two bonds to water, O$_w$. These two sodium cations are separated by only about 3.1 Å. Similarly, short Na–Na distances have been observed in both framework compounds and POM sodium salts.[47–49] (Na5–Na6 and Na11–Na12 are also ∼3.1 Å apart.) As mentioned previously, other phases containing the niobate lacunary cluster type cannot be made with any other alkali cations such as potassium, although in prior studies, both sodium and potassium have been successfully employed as counterions for dodecaniobate Keggin ion phases.[3–5] This suggests that perhaps the sodium cation

(44) Acerete, R.; Server-Carrio, J. *J. Am. Chem. Soc.* **1990**, *112*, 9386–9387.
(45) Cruywagen, J. J.; Vandermerwe, I. F. J.; Nassimbeni, L. R.; Niven, M. L.; Symonds, E. A. *J. Crystallogr. Spectrosc. Res.* **1986**, *16*, 525–535.
(46) Evans, H. T.; Rollins, O. W. *Acta Crystallogr., Sect. B* **1976**, *32*, 1565–1567.
(47) He, J.-H.; Wang, X. H.; Chen, Y.-G.; Liu, J.-F.; Hu, N.-H.; Jia, H.-Q. *Inorg. Chem. Commun.* **2002**, *5*, 796–799.
(48) Shikano, M.; Kremer, R. K.; Ahrens, M.; Koo, H.-J.; Whangbo, M.-H.; Darriet, J. *Inorg. Chem.* **2004**, *43*, 5–7.
(49) Belharouak, I.; Gravereau, P.; Parent, C.; Chaminade, J. P.; Lebraud, E.; Flem, G. L. *J. Solid State Chem.* **2000**, *152*, 466–473.

Table 5. ^{23}Na Quadrupole Coupling Constants (C_Q), Asymmetry Parameters (η_Q), and Isotropic Chemical Shifts (δ_{iso}) for **1**

site	P_Q (MHz)[a]	P_Q (MHz)[b]	C_Q (MHz)[c]	η_Q	δ_{iso} (ppm)[d]	δ_{3Q} (ppm)[e]
1	0.58 ± 0.04	0.66	0.63 ± 0.05	0.4 ± 0.1	3.1 ± 0.2	5.3 ± 0.3
2	2.0 ± 0.2	2.0	1.9 ± 0.1	0.4 ± 0.1	-3.1 ± 0.5	5.3 ± 0.3
3	2.1 ± 0.2	2.0	2.0 ± 0.1	0.0 ± 0.1	-5.3 ± 0.5	2.9 ± 0.3
4	2.4 ± 0.2	2.2	2.2 ± 0.1	1.0 ± 0.1	-8.4 ± 0.5	0.1 ± 0.3
5	1.7 ± 0.2	1.5	1.5 ± 0.1	0.1 ± 0.1	-5.8 ± 0.5	-3.6 ± 0.3

^{a} Calculated from eq 1 based on δ_{iso} and δ_{3Q}. ^{b} Calculated from eq 1 based on 2D fitting results. ^{c} Extracted from the 2D fit. ^{d} Extracted from a fit of a 1D slice taken along the F1 dimension. ^{e} Obtained from the 2D spectrum directly.

plays an important role in templating the formation of this cluster geometry.

The 1D ^{23}Na MAS NMR spectrum of **1** is depicted in Figure 6a. Multiple overlapping resonances are observed with low-intensity spinning side bands indicative of second-order quadrupolar broadening. A ^{23}Na MQ-MAS NMR spectrum was obtained that resolves five distinct Na sites, in agreement with the X-ray diffraction data (see Figure 6b). The ability to observe the different distinct Na environments demonstrates that the cations in this material do not undergo significant exchange and that the local coordination environments are not highly fluxional. There is some slight variation of the 1D ^{23}Na MAS NMR spectrum with reduction in temperature (down to 253 K, data not shown), suggesting minor variations in the average Na coordination environment with sample cooling. The quadrupolar parameters were extracted from the MQ-MAS spectrum by fitting the 2D spectrum. First, individual slices along the F1 dimension in the 2D spectrum were fit to obtain estimates of C_Q, η_Q, and δ_{iso} for each site. These parameters were used in an initial attempt to fit the complete ^{23}Na MQ-MAS 2D NMR spectrum (see Figure 6c,d). δ_{iso} can be used with the triple-quantum shift (δ_{3Q}) to calculate the quadrupolar product P_Q with the following equation:

$$\delta_{3Q} = \frac{17}{8}\delta_{iso} + \frac{1}{32}\frac{P_Q^2}{\nu_L^2} \times 10^6 \qquad (1)$$

where ν_L is the Larmor frequency and $P_Q = C_Q(1 + \eta_Q^2/3)^{1/2}$.[50-52] This relationship was used as a check for comparison with the parameters extracted from the full 2D fit. Excellent agreement is observed when comparing the values of P_Q obtained from the fit and those calculated with eq 1 (see Table 5). Additionally, distributions in both δ_{iso} and P_Q improve the fit of the 2D MQ-MAS experiment, again demonstrating that, while five distinct Na environments exist, there are minor local variations in the individual coordination environments, leading to these observed distributions. This again is in agreement with the X-ray data in that 15 crystallographically distinct Na sites were found. A complete analysis of the ^{23}Na NMR parameter distributions in comparison to the thermal parameters of the crystal structure is beyond the scope of this paper.

Assignment of the ^{23}Na MQ-MAS NMR spectrum is the focus of ongoing work. Ab initio calculations of the ^{23}Na

NMR chemical shift and electrical field gradient (EFG) using a DFT B3LYP 6-311++G(2d,2p) basis set and the level of theory for simple Na-centered clusters incorporating only the hydrogen-terminated nearest-neighbor oxygen, phosphorus, and sodium coordination environments have been obtained using the *Gaussian* software package.[53] Unfortunately, these results were inconclusive and did not allow for the assignment of the different environments. Previous ab initio studies of ^{23}Na NMR parameters by Tossell and co-workers[54] have shown that no simple relationship between the coordination number, the Na−O bond lengths, and the experimental ^{23}Na NMR parameters was observed. In addition, they have shown that the influence of other long-range cation interactions plays a significant role in the ^{23}Na NMR shielding. Our initial calculations involving larger Na-centered clusters by the incorporation of the Nb nuclei have been complicated by the influence of Nb on the calculated ^{23}Na NMR parameters. Surprisingly, the basis set and effective core potential previously used for Nb had a major impact on the calculated ^{23}Na NMR chemical shifts, EFG, and relative ordering. These basis set effects plus the use of different electrostatic models to overcome these difficulties[55] will be presented in a future paper. Unfortunately, this precludes the use of ab initio calculations for the direct assignment of the different Na environments in **1**. However, some preliminary assignments of the 15 general Na environments can be made based on the relative symmetry of the local Na environments. The Na$^+$ coordinated to six water molecules (Na2 and Na7) can be assigned to site 1 in Figure 6c. This assignment is justified by the very symmetric octahedral environment with six Na−O$_w$ bond lengths of ~2.4 Å. This environment is predicted to result in a small C_Q and the most positive isotropic chemical shift.[54] The assignment of the remainder of the sodium environments is not currently feasible because the effect of bridging Nb−O$_b$−Nb and Nb−O$_b$−P versus non-bridging (terminal) Nb−O$_t$ and P−O$_t$ oxygens, along with

(50) Frydman, L.; Harwood, J. S. *J. Am. Chem. Soc.* **1995**, *117*, 5367.
(51) Massiot, D.; Touzo, B.; Trumeau, D.; Coutures, J. P.; Virlet, J.; Florian, P.; Grandinetti, P. J. *Solid State Nucl. Magn. Reson.* **1996**, *6*, 73.
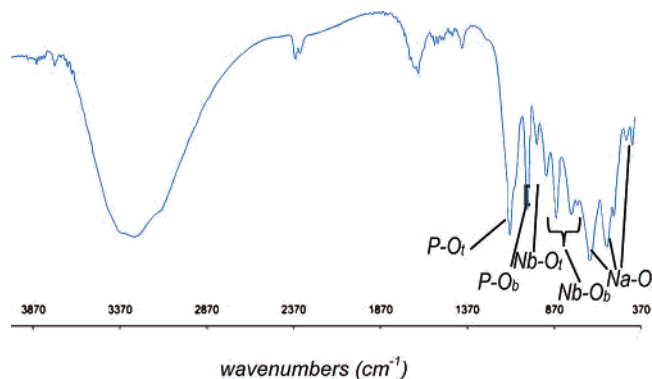(52) Medek, A.; Harwood, J. S. *J. Am. Chem. Soc.* **1995**, *117*, 12779.
(53) Frisch, M. J.; Trucks, G. W.; Schlegel, H. B.; Scuseria, G. E.; Robb, M. A.; Cheeseman, J. R.; Zakrezewski, V. G.; Montgomery, J. A.; Stratmann, R. E.; Burant, J. C.; Dapprich, S.; Millam, J. M.; Daniels, A. D.; Kudin, K. N.; Strain, M. C.; Farkas, O.; Tomasi, J.; Barone, V.; Cossi, M.; Cammi, R.; Mennucci, B.; Pomelli, C.; Adamo, C.; Clifford, S.; Ochterski, J.; Petersson, G. A.; Ayala, P. Y.; Cui, Q.; Morokuma, K.; Malick, D. K.; Rabuck, A. D.; Raghavachari, K.; Foresman, J. B.; Cioslowski, J.; Ortiz, J. V.; Stefanov, B. B.; Liu, G.; Liashenko, A.; Piskorz, P.; Komaromi, I.; Gomperts, R.; Martin, R. L.; Fox, D. J.; Keith, T.; Al-Laham, M. A.; Peng, C. Y.; Nanayakkara, A.; Gonzalez, C.; Challacombe, M.; Gill, P. M. W.; Johnson, B.; Chen, W.; Wong, M. W.; Andres, J. L.; Gonzalez, C.; Head-Gordon, M.; Replogle, E. S.; Pople, J. A. *Gaussian*, A.6 ed.; Gaussian, Inc.: Pittsburgh, PA, 1998.
(54) Liu, Y.; Tossell, J. A.; Nekvasil, *Am. Mineral.* **2004**, *89*, 1314−1322.
(55) Di Fiori, N.; Orendt, A. M.; Caputo, M. C.; Ferraro, M. B.; Facelli, J. C. *Magn. Reson. Chem.* **2004**, *42*, S41−S47.

Figure 7. Infrared spectrum of **1**.

the importance of Nb−O$_b$−Nb and Nb−O$_b$−P bond angles, on the ^{23}Na NMR parameters has not been fully explored. The impact of nonbridging oxygens or the oxygen type has been investigated for other oxides (Si−O−Si versus Si−O−Al) and shown to be significant.[54] Assignment of the other four Na$^+$ environments is currently being pursued and will be presented elsewhere.

Last, infrared spectroscopy was used to characterize **1** in the solid state and to identify fingerprint peaks of heteropolyniobates, and the spectrum is shown in Figure 7. Peak assignments are made primarily by comparison to infrared studies on other PO$_4$-centered Keggin ions and lacunary derivatives. The two peaks at 1120 and 1025 cm^{-1} are assigned to P−O$_t$ and P−O$_b$, respectively (t = terminal and b = bridging).[56−58] The three decorating phosphates, P1, P2, and P3, have two short P−O$_t$ bonds each, around 1.52 Å in length. Both the decorating and central phosphates have longer P−O$_b$ bonds that are 1.56−1.57 Å for the decorating phosphates and 1.52−1.55 Å for the central phosphate. M−O$_t$ bonds (M = Mo and W) of molybdate and tungstate Keggin ions are assigned to vibrational frequencies between 900 and 1000 cm^{-1}, and M−O$_b$ vibrations are assigned to peaks generally between 700 and 900 cm^{-1} by Thouvenot et al.[56] In the [(PO$_2$)$_3$PNb$_9$O$_{34}$]$^{15-}$ anion, we have three types of Nb−O$_b$ sites: between two corner-sharing NbO$_6$ octahedra, between two edge-sharing NbO$_6$ octahedra, and corner-sharing between a NbO$_6$ and a decorating PO$_4$. Therefore, we observe multiple sharp peaks for vibration of these different O$_b$ environments (see Figure 7). The peaks below 700 cm^{-1} in the spectrum of **1** are assigned to Na−O vibrational modes of the sodium cations bonded to the

polyanion clusters and water molecules. This assignment is made in that these peaks are absent in the spectrum of **1**, which has undergone ion exchange of the sodium for ammonium surfactants (the subject of a future publication), correlating with >98% removal of Na$^+$, as determined by ^{23}Na MAS NMR. Finally, the broad band centered around 3200 cm^{-1} is the O−H stretch of lattice water.

Conclusions

We report the solid-state characterization of a new heteropolyniobate phase composed of decorated A-type trivacant lacunary α-Keggin ions [(PO$_2$)$_3$PNb$_9$O$_{34}$]$^{15-}$ that are linked into a rigid and poorly soluble framework by their charge-balancing sodium cations. This phase represents the first true lacunary heteropolyniobate and the first PO$_4$-centered heteropolyniobate reported. Characterization by ^{23}Na NMR showed remarkable spectroscopic resolution of the sodium sites, confirming that these sodium cations behave more as linking ions in a rigid framework rather than mobile, hydrated species that are more typical of a hydrated form of an ionic salt. Future work on this phase will involve the development of a computational model that accurately simulates the ^{23}Na NMR spectrum. This work will be applied specifically for a more rigorous peak assignment of the ^{23}Na NMR spectrum of **1** and for use in interpreting ^{23}Na NMR spectra of similar Na salts of heteropolyniobates and, more generally, for interpretation of ^{23}Na NMR spectra of solid-state phases that contain sodium in rigid and well-defined framework sites. Future and current work on this phase and other linked heteropolyniobate phases involves the use of an ammonium surfactant to disrupt the linked framework to form ordered arrays of isolated clusters and surfactant molecules.

Supporting Information Available: Crystallographic file (CIF), a high-speed ^{1}H MAS NMR spectrum and a DQ-filtered ^{1}H MAS NMR spectrum of **1**, and ^{1}H → ^{31}P CP buildup curves for **1**. This material is available free of charge via the Internet at http://pubs.acs.org.

IC051155G

(56) Thouvenot, R.; Fournier, M.; Franck, R.; Rocchiccioli-Deltcheff, C. *Inorg. Chem.* **1984**, *23*, 598−605.
(57) Moore, B.; Foger, K. *Inorg. Chim. Acta* **1991**, *181*, 201−205.
(58) Moustafa, Y. M.; El-Egili, K. *J. Non-Cryst. Solids* **1998**, *240*, 144−153.